NIH Public Access
Author Manuscript
*Arch Pathol Lab Med*. Author manuscript; available in PMC 2013 May 01.

Published in final edited form as:
*Arch Pathol Lab Med*. 2012 May ; 136(5): 517–526. doi:10.5858/arpa.2011-0147-OA.

# Multiphoton microscopy in the evaluation of human bladder biopsies

**Manu Jain**[1,#], **Brian D. Robinson**[1,2,#], **Douglas S. Scherr**[1], **Joshua Sterling**[3], **Ming-Ming Lee**[1], **James Wysock**[1], **Mark A. Rubin**[2], **Frederick R. Maxfield**[3], **Warren R. Zipfel**[4], **Watt W. Webb**[5], and **Sushmita Mukherjee**[3,*]

[1]Department of Urology, Weill Cornell Medical College, New York, NY

[2]Department of Pathology and Laboratory Medicine, Weill Cornell Medical College, New York, NY

[3]Department of Biochemistry, Weill Cornell Medical College, New York, NY

[4]Department of Biomedical Engineering, Cornell University, Ithaca, NY

[5]School of Applied and Engineering Physics, Cornell University, Ithaca, NY

## Abstract

**Context—**Multiphoton microscopy (MPM) is a nonlinear imaging approach, providing cellular and subcellular details from fresh (unprocessed) tissue by exciting intrinsic tissue emissions. With miniaturization and substantially decreased cost on the horizon, MPM is an emerging *in vivo* imaging technique with many potential clinical applications.

**Objective—**To assess the imaging ability and diagnostic accuracy of MPM for human bladder biopsies.

**Design—**Seventy-seven fresh bladder biopsies were imaged by MPM and subsequently submitted for routine surgical pathology diagnosis. Twelve cases were excluded due to extensive cautery artifact that prohibited definitive diagnosis. Comparison was made between MPM imaging and gold standard hematoxylin and eosin (H&E) stained sections of each specimen.

**Results—**In 57/65 cases (88%), accurate MPM diagnoses (benign or neoplastic) were given based upon the architecture and/or cytologic grade. The sensitivity and specificity of MPM in our study were 90.4% and 76.9%, respectively. A positive (neoplastic) diagnosis on MPM had a high predictive value (94%), and negative (benign) diagnoses were sustained on histopathology in two-thirds of cases. Architecture (papillary vs. flat) was correctly determined in 56/65 cases (86%), and cytologic grade (benign/low vs. high grade) was assigned correctly in 38/56 cases (68%).

**Conclusions—**MPM images alone provide sufficient detail to classify most lesions as either benign or neoplastic using the same basic diagnostic criteria as histopathology (architecture and cytologic grade). Future developments in MPM technology may provide urologists and pathologists with additional screening and diagnostic tools for early detection of bladder cancer. Additional applications of such emerging technologies warrant exploration.

## INTRODUCTION

The American Cancer Society estimated that 70,530 new cases of bladder cancer were diagnosed in 2010 in the United States alone, accounting for 14,680 deaths.[1] Bladder cancer

*Address correspondence to: Sushmita Mukherjee, PhD, MS, Department of Biochemistry, Room E 019A, Weill Cornell Medical College, 1300 York Avenue, New York, NY 10065.
#These authors contributed equally to the study

NIH-PA Author Manuscript
NIH-PA Author Manuscript
NIH-PA Author Manuscript

NIH-PA Author Manuscript

NIH-PA Author Manuscript

NIH-PA Author Manuscript

ranks as the fourth most common malignancy and ninth leading cause of death from cancer in men, who are nearly three times more likely to develop bladder cancer as compared to women.[1] The urothelium is the dominant type of epithelium lining the urinary bladder, ureters, and the renal pelvis, and more than 90% of bladder cancers are urothelial carcinomas.[2, 3] The World Health Organization (WHO) 2004/International Society of Urological Pathology (ISUP) classification of bladder lesions includes the following three broad diagnostic categories: (1) flat intraurothelial lesions (ranging from benign to malignant), (2) papillary urothelial lesions (ranging from benign to malignant), and (3) invasive urothelial neoplasms (low grade and high grade).[2, 4]

Approximately 70% of newly diagnosed cases of bladder cancer represent superficial disease, *i.e.*, non-muscle-invasive (pathologic stage Ta, T1 or Tis).[3, 5] The natural history of these superficial bladder cancers is difficult to predict because of tumor heterogeneity and multifocality, and these patients are prone to disease recurrence and progression. The recurrence and progression rates of superficial bladder cancer vary according to several tumor characteristics, mainly tumor grade, stage, and the presence or absence of carcinoma *in situ* (CIS).[2, 5-7] Urothelial papillomas, papillary urothelial neoplasms of low malignant potential (PUNLMP), and non-invasive low grade papillary urothelial carcinomas have a low rate of disease progression, whereas all superficial high grade urothelial carcinomas, whether flat or papillary, are at high risk for progression.[3, 7, 8]

Early detection, diagnosis and treatment of these superficial bladder cancers would improve prognosis and possibly provide a cure for some patients. However, current diagnostic techniques, namely urine cytology and white light cystoscopy, are unable to provide optimal sensitivity and specificity for early stage bladder cancers—especially CIS—resulting in compromised patient care.[9] For instance, patients with suspicious or positive urine cytology but no obvious tumor during cystoscopic exam may be subjected to numerous (including many benign) biopsies in order to rule in or out carcinoma. Not infrequently, these patients must undergo repeat cystoscopy and biopsy when all initial biopsies are non-diagnostic or negative for carcinoma. Cystoscopy and biopsy procedures are not without potential complications, such as bleeding, infection, and, occasionally, bladder perforation. In addition, repeat cystoscopy after non-diagnostic procedures increases both direct and indirect health care costs and negatively impacts patient quality of life.[10, 11]

High magnification, high resolution “optical biopsy” techniques, such as multiphoton microscopy (MPM), are currently being explored as alternative and adjunctive approaches to diagnosis. MPM relies on the simultaneous absorption of two (or three) low energy (near-infrared) photons to cause a nonlinear excitation equivalent to that created by a single photon of bluer light. Excitation only occurs where there is sufficient photon density (*i.e.*, at the point of laser focus), providing intrinsic optical sectioning with resolution equivalent to traditional confocal microscopy. Tissue penetration is greater than with standard confocal microscopy because absorption and scattering of the laser excitation is reduced at near-infrared wavelengths compared to the visible or ultraviolet region of the spectrum.[12, 13]

Most importantly, by utilizing two-photon excitation in the 700-800 nm range, MPM enables both *in vivo* imaging as well as *ex vivo* imaging of fresh, unprocessed and unstained tissue via intrinsic tissue emissions (ITEs). The ITE signal is composed of two components: (i) tissue autofluorescence, in part from reduced nicotinamide adenine dinucleotide (NADH) and flavin adenine dinucleotide (FAD) in cells, elastin in the connective tissue, and lipofuscin in fat and other cells, and (ii) second harmonic generation (SHG), a nonlinear scattering signal which arises from non-centrosymmetric structures such as tissue collagen.[12-14] It has been shown that MPM/ITE imaging is capable of generating distinctive optical signals that enable imaging of animal[13] and human[15-17] tissues at sub-micron

NIH-PA Author Manuscript

NIH-PA Author Manuscript

NIH-PA Author Manuscript

resolution in three dimensions to a depth of up to 0.5 mm below the specimen surface, at acquisition rates of ~1 image/second, with $>10^5$ pixels per image. These imaging parameters enable detailed visualization of cellular and subcellular structures, which is important because changes in cellular and subcellular morphology accompany the development of pre-cancerous lesions and cancers.[18]

With *in vivo* MPM imaging techniques currently under investigation for assessment of pulmonary and other solid tumors, application of MPM to bladder or other hollow viscera is likely soon to follow. However, in order for MPM to become a clinically useful adjunct tool, it is essential to assess the ability of MPM to identify relevant bladder lesions as compared to the current gold standard hematoxylin and eosin (H&E) stained thin section histopathology. Here, we report a prospective study of 77 human bladder biopsies that were first imaged (fresh, unfixed, and unstained) with MPM, and then processed for routine H&E histopathology. MPM images were read by two trained surgical pathologists, and those diagnoses were compared to final histopathology results. Our results suggest that MPM image sets alone obtained from these unprocessed biopsies can readily distinguish between normal bladder mucosa, benign inflammatory/reactive lesions, CIS, papillary urothelial carcinomas, and, to a lesser degree, invasive urothelial carcinomas. These observations indicate that MPM could be an important potential tool to provide immediate "intra-cystoscopic" diagnostic impressions that can guide urologists in biopsy and patient management.

## MATERIALS AND METHODS

### Study Cohort

The study included 77 adult men and women who reported to the clinical urology practice at Weill Cornell Medical College, New York, NY with symptoms and cystoscopic findings consistent with bladder cancer and who were scheduled for a trans-urethral resection of bladder tumor (TURBT). All subjects were consented to participate in an Institutional Review Board (IRB) approved study to image with MPM one of their biopsies before it was submitted to Surgical Pathology for diagnostic histopathologic examination. The nature of the detour of one of their biopsies to the MPM facility for one hour, before going to surgical pathology, was clearly explained to the subjects before consent was taken. Specimens for MPM were collected only from cases where a sufficient number of biopsies had been obtained to ensure that diagnostic ability was not compromised due to participation in the research study.

### Multiphoton Microscopy

**Specimen acquisition and handling—**Seventy-seven fresh bladder biopsy specimens, obtained from TURBT or cold cup biopsies, were imaged with MPM. Immediately after excision, the specimens were collected in bottles containing normal saline, placed on ice, and brought directly to the MPM facility for imaging. Immediately after MPM imaging (up to a maximum of one hour), the specimens were placed in 10% buffered formalin and submitted for routine histopathology.

**Specimen imaging—**In the MPM imaging facility, each biopsy specimen was placed on a small tissue culture dish with a central well, with the urothelium oriented upwards. The specimen was then imaged using a custom-built MPM system consisting of an Olympus BX61 upright microscope (Olympus America, Center Valley, PA) and a modified Bio-Rad 1024 scan-head (Bio-Rad, Hercules, CA). Images were acquired at two magnifications: (i) low magnification for overall architectural information (4X, 0.28 NA Olympus dry objective), allowing imaging of 3.1 $mm^2$ frames at 6 μm/pixel resolution and (ii) high

NIH-PA Author Manuscript

NIH-PA Author Manuscript

NIH-PA Author Manuscript

magnification for detailed cellular and local architectural information (20X, 0.95 NA Olympus water-immersion objective), allowing imaging of 614 $\mu m^2$ frames at 1.2 $\mu m$/pixel resolution. If necessary, higher scanner (digital) zooms were used for further magnification. When imaging with the 20X water immersion objective, a cover slip was placed on a normal buffered saline-moistened biopsy, and a drop of normal saline was placed on the cover slip to achieve water immersion. The specimens were excited using a tunable Ti-Sapphire laser (Mai Tai, Spectra-Physics Lasers, Newport Corp., Irvine, CA) tuned to 780 nm. The pulse width at the sample was estimated to be ~160 fs when delivered through the 4x macro lens and ~200 fs through the 20x objective, based on pulse autocorrelation measurements made on an identical MPM system. The laser power was controlled through a Pockels Cell (Conoptics, Danbury, CT) and typically used a maximum power of 60-80 mW when acquiring data with the 20x/0.95 water immersion objective. Images were collected in two channels: (i) second harmonic generation (SHG) signal centered at 390 nm (±35 nm) and (ii) broadband autofluorescence at 420–530 nm.

Typically, the collection of each image frame shown in the figures took 1-3 sec. Imaging through all the optical sections of a given area (20-40 images) took 1 – 1.5 min. The images can be evaluated by a pathologist during image acquisition. No post-processing is necessary to identify essential architectural and cellular features.

**MPM image evaluation—**All images were obtained as stacks of optical sections up to a tissue depth of 0.5 mm with the 4X objective and ~0.25 mm with the 20X objective. For better appreciation of the structures, the raw 8-bit grayscale images were color-coded red for SHG signals and green for autofluorescence signals. The two pathologists independently reviewed all MPM images, categorizing each lesion based on (i) architecture and (ii) cytologic grade. These were scored numerically, as described in the section on data analysis below. The specific diagnostic criteria used in MPM, as compared to standard histopathology, are provided in Table 1.

One of the pathologists began the project earlier and had a training period of three months, where she compared previously acquired MPM image sets with H&E slides from the same cases (not included in this study). The second pathologist, on the other hand, had a relatively brief “training phase,” where he reviewed 10 comparative MPM and H&E image sets with the first pathologist, representing all classes of lesions included in this study.

## Histopathology

After MPM imaging, the biopsies were processed per standard protocol in the Surgical Pathology laboratory [*i.e.*, formalin fixation, paraffin embedding, 5-$\mu m$ thick sectioning, and H&E staining, briefly referred to as formalin-fixed, paraffin-embedded (FFPE) specimens]. Cases were diagnosed by the attending pathology staff at Weill Cornell Medical College and reported using the WHO/ISUP (2004) grading system, with lesions classified into benign lesions (including reactive conditions, such as *cystitis cystica*), CIS, non-invasive papillary urothelial carcinoma (low and high grade), and invasive carcinoma.

## Data Analysis

All MPM diagnoses were scored by the two pathologists as follows. Architectural diagnoses: flat = 1, favor flat = 2, favor papillary = 3, or papillary = 4. Similarly, cytologic grade was reported as: benign/low grade = 1, favor benign/low grade = 2, favor high grade = 3, or high grade = 4. MPM diagnoses were then compared to the gold standard histopathology diagnoses given by the attending pathologists, which were also coded numerically by the two pathologists using precisely the same scoring system described above for MPM diagnoses.

NIH-PA Author Manuscript

NIH-PA Author Manuscript

NIH-PA Author Manuscript

The following diagnostic criteria were evaluated: (1) ability to accurately diagnose neoplastic processes and (2) ability to accurately diagnose cytologic grade of lesions. All cases that obtained scores of 1 or 2 for *both* architecture and grade were classified as "benign" and those that obtained a score of 3 or 4 in either architecture or grade were classified as "neoplastic." Regarding cytologic grade, all cases that obtained a grade of 1 or 2 were classified as "benign/low grade" and those that obtained a score of 3 or 4 were classified as "high grade".

Statistical testing used a standard 2×2 contingency table comparing MPM with gold standard H&E histopathology in order to determine the diagnostic test operating characteristics (accuracy, sensitivity, specificity, positive predictive value, and negative predictive value), as shown in Figure 1.

Visual comparisons were also made between images obtained from MPM image sets and the H&E slides of the corresponding bladder biopsy tissue, with the goal of identifying correlates and discrepancies in diagnosis, understanding the advantages and disadvantages of MPM, and for proposing MPM instrumentation improvements that would improve diagnostic accuracy.

## RESULTS

Based on MPM images obtained at low magnification, we were able to differentiate flat (non-papillary) lesions from papillary lesions. Based on cytologic features (*i.e.*, nuclear-to-cytoplasmic or N:C ratio, polarity, and nuclear pleomorphism) obtained from MPM images at high magnification, we were able to grade papillary tumors as either low or high grade, and flat lesions were categorized into benign/reactive or CIS.

### Flat Intraurothelial Lesions and Invasive Urothelial Carcinoma

**Normal bladder histology and benign/reactive lesions—**At low magnification (Figure 2A, 2B), the flat (non-papillary) nature of the lesions was evident in benign urothelium. The unique structure of the urothelium, with its multiple (3-7) cell layers and surface umbrella cells, was recognized based on the cellular autofluorescence signal (color-coded green) at higher magnification. A higher magnification of the umbrella cells is shown in the inset of Figures 2C and 2D. The underlying lamina propria consisted of collagen fibers, which generate SHG signal (color-coded red), interspersed with wavy, autofluorescent elastin fibers (color-coded green). These distinct signals allowed us to clearly identify features corresponding to normal bladder histology and to identify the junction of urothelium and lamina propria. Von Brunn nests in lamina propria, including *cystitis cystica* (Figure 2E, 2F; arrow), were similarly straightforward to identify.

**Flat Carcinoma in situ (CIS)—**In contrast to benign urothelium, where cells have columnar to ovoid nuclei oriented perpendicular to the basement membrane, biopsies with CIS showed flat urothelial lining and characteristic loss of polarity at low magnification (Figure 3A, 3B). At higher magnification (Figure 3C, 3D), CIS was diagnosed on the basis of high grade cytologic atypia, that is, large cells with marked pleomorphism and high N:C ratio (arrows).

**Invasive urothelial carcinoma—**All cases of invasive urothelial carcinomas in this study (n=7) were high grade lesions. Invasion into lamina propria ranged from minimal to extensive, and two cases showed muscularis propria invasion. Most of these biopsies, however, were superficial in nature, and muscularis propria was not present. One case could not be evaluated for invasion by MPM due to lack of available high magnification images. Lamina propria invasion was identified by MPM in only one out of the remaining six

NIH-PA Author Manuscript

NIH-PA Author Manuscript

NIH-PA Author Manuscript

invasive carcinoma cases. This case (Figure 3F) showed extensive invasion on light microscopic examination. At low magnification on MPM we could appreciate clusters and nests of autofluorescent urothelial carcinoma cells (coded green; Figure 3Ea, 3Fa) infiltrating the SHG-signal-rich collagen bundles (coded red; Figure 3Eb, 3Fb) within the lamina propria. For the most part, however, invasion was difficult to assess by MPM. For instance, MPM did not provide sufficient information to identify microinvasion into lamina propria or invasion in cases with extensive cautery artifact. These limitations were due to the relatively small field and depth of view possible using the current MPM apparatus, as well as the low statistical probability of detecting microinvasion on any given section. Nevertheless, all six evaluable cases of invasive urothelial carcinoma were correctly identified on MPM as being high grade neoplastic processes, whether invasion was detected or not.

### Noninvasive Papillary Urothelial Carcinoma

At low magnification, the papillary nature of the urothelium was appreciated in all papillary urothelial neoplasms (Figures 4A, 4B and 5A, 5B). The complex, arborizing papillae are composed of thin fibrovascular cores containing collagen fibers (SHG signal, color-coded red) and lined by a thickened epithelial layer (autofluorescence, color-coded green). In some cases, the papillary cores become hyalinized, which can be seen as reddish homogeneous areas on MPM (Figure 5E, 5F).

The N:C ratio and degree of pleomorphism, seen at higher magnification, were evaluated in differentiating papillary lesions into low and high grade urothelial carcinomas.

**Low grade papillary urothelial carcinomas—**Low grade papillary lesions had thickened but orderly urothelium (color-coded green), sometimes appearing fused, and papillary fronds with thin fibrovascular cores (color-coded red; Figure 4A, 4C, 4D; arrows). At higher magnification, low grade papillary urothelial carcinomas showed only mild variation in nuclear size and shape, with an overall low N:C ratio (Figure 4E, 4F).

**High grade urothelial carcinomas—**High grade papillary urothelial carcinomas had similar low power architecture as the low grade papillary carcinomas, showing thickened papillary fronds that more frequently fused, forming sheets of tumor cells between the fronds (Figure 5A-5F). At higher magnification, these cells showed moderate to marked nuclear pleomorphism and high N:C ratio (Figure 5E, 5F).

### Assessment of MPM as a diagnostic tool

The distribution of the 65 cases evaluated were as follows: (1) Benign urothelium (including reactive) = 13; (2) CIS = 14; (3) Papillary low grade urothelial carcinoma = 17; (4) Papillary high grade urothelial carcinoma = 14; and (5) Invasive urothelial carcinoma = 7.

The diagnostic accuracy of MPM was 88% (57 total accurate diagnoses, including 47 neoplastic and 10 benign). Three cases were called neoplastic on MPM that were diagnosed as benign on H&E, and 5 cases were called benign on MPM but showed neoplastic features on final FFPE pathologic examination. Overall, MPM showed a sensitivity of 90%, specificity of 77%, positive predictive value of 94%, and a negative predictive value of 67% as shown in Figure 1. The architecture of the lesion (flat or papillary) was correctly defined using MPM in 86% of cases. Determination of cytologic grade was accurate using MPM in 38 of 56 (68%) of cases. Nine cases had to be excluded from the grading by MPM, since these data sets had certain intrinsic limitations. Specifically, 6 cases lacked high magnification images, 2 cases had specimens with largely denuded epithelium, and 1 case had a degree of cautery that allowed architectural analysis but not grading.

NIH-PA Author Manuscript

NIH-PA Author Manuscript

NIH-PA Author Manuscript

As discussed in the Methods (section titled “MPM image evaluation”), the training phase of the pathologists was quite brief. Even with this brief training, both pathologists agreed in their classification of lesions as benign or neoplastic in all 65 cases (100% concordance). They also agreed on the architecture of the lesion (flat versus papillary) in all cases. In only three of fifty-six cases (5%) was there discordance in the grading of lesions (benign/low grade versus high grade), and all three of these cases were non-invasive papillary urothelial carcinomas.

## DISCUSSION

MPM image sets examined using ITE signals alone from fresh tissue can provide high-magnification, high-resolution images of fresh human bladder biopsies allowing a high degree of diagnostic accuracy. In our study, we could identify benign bladder mucosa and submucosa by the flat architecture, bland urothelium (including superficial umbrella cells), and underlying lamina propria (including blood vessels and von Brunn nests). Furthermore, benign mucosa was distinguishable from flat CIS using cytologic detail apparent at high magnification. In fact, many of the same criteria used in light microscopic examination of H&E sections to diagnose CIS are present and evaluable in MPM (*e.g.*, N:C ratio, pleomorphism, polarity). Invasive carcinoma was also identifiable using MPM, though more rarely, where irregular nests of malignant urothelial cells could be seen infiltrating collagen fibers of the lamina propria.

Papillary lesions could be identified by the frondular structures that define these lesions, and further classification into low grade and high grade tumors was feasible using cytologic details at high magnification, similar to the differentiation possible between benign flat mucosa and flat CIS.

In addition to carcinomas, a variety of benign lesions were readily identifiable by MPM that may appear cystoscopically suspicious for carcinoma, including *cystitis cystica* and florid proliferation of von Brunn nests.

It is also important to note that even with only a brief training phase, the two pathologists agreed on the classification of specimens as either benign or neoplastic in all cases. Similarly, architectural classification of lesions was identical between the two pathologists. A high level of concordance was seen in the interobserver grading of lesions, such that discrepancy in grading occurred in only three cases of non-invasive papillary urothelial carcinoma. The high level of concordance with relatively minimal training is likely due, at least partially, to the strong similarities between MPM images and standard histopathologic examination of FFPE tissue.

Current methods used in pathology to offer immediate impressions and evaluate specimen adequacy, such as frozen section analysis and Diff-Quick® examination of fine needle aspirations, introduce irreversible freezing[19] and air-drying artifacts, respectively, often making a definitive final diagnosis on that specimen nearly impossible. For this reason, biopsy specimens are not routinely subjected to frozen section analysis since these small specimens may contain the suspicious lesion in its entirety. MPM, on the other hand, introduces no artifacts during processing, and subsequent FFPE H&E sections of MPM-imaged tissue are indistinguishable from non-MPM-imaged tissue. Thus, MPM offers the ability to assess biopsy adequacy, *ex vivo* currently--and *in vivo* in the near future--without altering the tissue for permanent section diagnosis and ancillary analyses (e.g., immunohistochemistry).

We expect the initial translation of MPM into the cystoscopy workflow to consist of fast, non-destructive *ex vivo* evaluation of excised biopsies to achieve, among other things, the

NIH-PA Author Manuscript

NIH-PA Author Manuscript

NIH-PA Author Manuscript

evaluation of biopsy adequacy in cases of suspected CIS, the confirmation of the presence of a papillary neoplasm, and, potentially, immediate diagnostic impressions to alleviate patient anxiety in awaiting results and expedite the scheduling of resection or other intravesical procedures in cases of carcinoma. The ability of MPM to provide real time diagnoses of benign entities such as *cystitis cystica* and proliferation of von Brunn nests could direct urologists in further evaluation and sampling of the patient with urine cytology suspicious or diagnostic of carcinoma.

In this study, we used a laboratory-based MPM system built for research applications. Using this system, the imaging time for a 1 $mm^3$ biopsy specimen, covering the entire specimen surface and imaging up to ~0.5 mm below the surface at low magnification (4x objective) and ~0.25 mm below the surface at higher magnification (20x objective), took ~20 minutes. While this time is already comparable with typical turn-around-time for frozen sections, there are significant technical developments occurring in the field that are expected to bring this time down by an order of magnitude or more in the near future.[20-24] Also, custom-designed MPM systems targeting a single type of clinical application will be more compact, cost-efficient, easy to operate and interpret, and usable as an *in vivo* tool, thus potentially preventing unnecessary benign biopsies. Such systems are already in existence and being tested for use in the lung, among other organs. These improvements and customizations to MPM could include, for example, replacing the tunable laser with a portable, single wavelength fiber laser; incorporating automated sample handling and automated analysis; maximizing microscopic detail while minimizing imaging time (e.g., by imaging the excised biopsy simultaneously from top and bottom), and providing a visual rendition of the images in a format most useful to the specific group of end users.

The use of MPM does have some limitations in its current state. For instance, MPM is able to image with meaningful contrast only up to 0.5 mm below the surface of human bladder tissue, which limits evaluation of lamina propria invasion. Muscularis propria evaluation is also limited for the same reason. Fortunately, many technological developments are on the horizon, which are expected to improve the penetration depth of MPM imaging (*e.g.*, dispersion compensation for maintaining the shortest possible laser pulse width at the specimen, adaptive optics to correct for aberrations, more efficient photodetectors, and new optics with better transmission profiles in the relevant wavelength regimes).

Another major limitation of MPM is that nuclei do not exhibit any ITE signals (autofluorescence or SHG) in the wavelength ranges used with the current imaging technique. Rather, they are seen as dark areas devoid of any signal. These dark areas, surrounded by autofluorescent (color-coded green) cytoplasm, still allow one to define the nuclear contour, and thereby the size of the nucleus and N:C ratio. However, intranuclear details, such as presence and size of nucleoli or the chromatin pattern, are indiscernible in MPM using ITE alone. This lack of intranuclear detail could pose significant problems, for instance, if the difference between dysplasia and CIS is necessary during cystoscopic examination. At least for *ex vivo* biopsy analysis, however, using exogenous nuclear stains such as acridine orange could largely circumvent this problem. In preliminary results using animal tissue (data not shown), we have obtained excellent staining of nuclei by incubation of several mm thick tissues with acridine orange for 15 sec at room temperature, followed by 2-3 buffered saline washes. Acridine orange fluoresces at the same excitation wavelength as used in the current study (780 nm), and, thus, can be easily combined with autofluorescence and SHG imaging. Such a staining protocol for biopsy analysis, if necessary, seems possible without a significant increase in time requirements.

Finally, current systems are prohibitively expensive for practical clinical application. Nevertheless, advances in the technology and design of these systems, as has occurred with

NIH-PA Author Manuscript

NIH-PA Author Manuscript

NIH-PA Author Manuscript

almost all new and emerging technologies, are expected to drastically decrease the costs. We feel that validation of adjunctive diagnostic and screening tools such as MPM should be tested in parallel to potential development of clinical utility, so that access to these systems is not delayed and patients may benefit from potential improved survival as well as quality of life.

Multiphoton imaging joins an array of other optical imaging techniques that are being assessed for real-time diagnosis and intra-surgical assistance. Specifically, two types of techniques are being assessed. The first category includes low magnification, large field of view "primary detection" or "red-flag" techniques, where the goal is to scan an entire organ, such as the bladder, for potentially suspicious lesions[25, 26]. Techniques in this category include: (a) photodynamic detection or fluorescence cystoscopy, where an exogenous contrast agent is instilled in the bladder to improve identification of neoplastic tissue over surrounding normal mucosa; and (b) narrow band imaging, where the mucosa is illuminated with narrow bands of blue and green light using optical filters. These wavelengths are preferentially absorbed by hemoglobin, generating better visualization of neoplastic vasculature and other mucosal pattern changes. These techniques typically have high sensitivity but low specificity, primarily because similar signals are generated by benign inflammatory lesions in addition to neoplasia.

This leads to the need for a second class of optical techniques, the so-called "targeted imaging" or "optical biopsy" techniques[25, 26]. Here, the field of view is typically smaller, but the images are of higher magnification and resolution, approaching those used for traditional post-procedure histopathology on excised tissues. It is expected that these techniques will work in conjunction with one or more red-flag technique(s), which will direct the specific areas sampled. Techniques in this category include Raman spectroscopy, optical coherence tomography (OCT) and confocal microendoscopy[25, 26]. Each of these techniques has unique advantages and limitations. Raman spectroscopy, as assessed clinically, is a non-imaging technique, where average Raman spectra are acquired from a relatively large area (~1 $mm^3$). However, this technique is able to assess specific chemical changes in the tissue and thereby diagnose neoplastic status. Raman spectroscopy has been evaluated in clinical trials for breast lumpectomy margin and atherosclerotic plaque assessments[27, 28]. To the best of our knowledge, it has not yet been studied in the context of bladder cancer assessments. OCT is a relatively mature technique[29] that has been assessed *in vivo* in transurethral procedures and has been found to improve the detection of early/flat urothelial lesions, especially when combined with fluorescence cystoscopy to identify areas to target[30]. Confocal microendoscopy has been used in the upper gastrointestinal tract to visualize Barrett's esophagus[31], and it has also been assessed in transurethral procedures, where it has been shown to be able to distinguish between normal urothelium and low- and high-grade tumors[32].

MPM has some advantages over both OCT and confocal microendoscopy. The latter technique requires instillation of a contrast agent (fluorescein) for imaging, whereas MPM can be contrast-free. Furthermore, since visible (blue) light is used for tissue illumination in confocal microendoscopy, depth of imaging is 2-3-fold shallower than MPM, which uses more penetrating near-infrared illumination. OCT, on the other hand, can image 2-5-fold deeper into tissue than MPM, but typically has a 5-20-fold lower lateral resolution. However, laboratory-based OCT systems are now available approaching resolutions similar to MPM. Furthermore, traditional OCT is carried out in B-mode, similar to ultrasound imaging, generating XZ images that are somewhat less intuitive for intra-procedural interpretation. This problem can be easily overcome, though, by automated image analysis and by adequate training of the endoscopist.

NIH-PA Author Manuscript

NIH-PA Author Manuscript

NIH-PA Author Manuscript

Given the limitations and complementary nature of these techniques, the ultimate clinical tool will likely be multimodal in nature, combining one or more red-flag and/or optical biopsy systems. As a stand alone tool, MPM currently offers the ability to make real-time diagnoses on excised tissue specimens without any processing of the tissue or introduction of permanent artifacts, such as those seen in tissue submitted for “frozen section” diagnosis. While this study focused on the urinary bladder, our experience suggests that an immediate impression/diagnosis can be given on tissue from a variety of organs, including the kidney, lung, and colon, among others. One use of the technology as is stands now, then, would be as an adjunct or alternative to frozen section analysis for immediate diagnoses. Another potential application would be the assessment of endoscopic biopsies for specimen adequacy for future FFPE diagnoses. Future developments will likely lead to introduction of MPM as an endoscopic technique, allowing optical biopsy of tissue *in vivo*. Several such attempts at miniaturization of MPM into endoscopic formats are currently in progress.[33-36] The MPM images generated may be streamed over a secure server to a consulting pathologist for assessment. Such an endoscopic “biopsy” tool would prove invaluable, for instance, in lesions of the upper urinary tract, where the capability of biopsying a suspicious focus is often limited by the ability to introduce and navigate the necessary instruments through the ureter and into the renal pelvis. An “optical biopsy” tool would also likely minimize the removal of unnecessary biopsies (e.g., inflammatory lesions) and allow mapping of carcinomatous areas to ensure complete resection, thereby streamlining and improving the throughput of surgical pathology workflow and, ultimately, optimize patient care.

In conclusion, we show that MPM image sets alone can readily distinguish between normal bladder mucosa, benign inflammatory/reactive lesions, CIS, papillary urothelial carcinomas, and, to a lesser degree, invasive urothelial carcinomas. The ability of MPM to diagnose early stage bladder carcinoma, and more specifically CIS, is important, especially since CIS is associated with poor prognosis and is frequently difficult to identify during routine cystoscopy. We expect that a future study with a larger sample size and utilization of the technical lessons learnt from this work (such as imaging larger areas, always acquiring both low and high magnification images, avoiding regions of cautery, etc.), will further improve our grading ability by MPM. We are currently planning a prospective study of the utility of MPM in individuals with abnormal urine cytology, where we will investigate the potential impact of immediate MPM diagnosis of a biopsy on the management and subsequent detection of bladder carcinoma. The initial evaluation will involve assessment of *ex vivo* biopsies in the cystoscopy suite to guide the urologist in assessing specimen adequacy in cases with a diagnosis of urothelial carcinoma on cytology. Meanwhile, new technological developments, such as miniaturization of MPM into endoscopic formats, as discussed above, are likely to bring “optical biopsies” into routine clinical use.

## References

1. Jemal A, Siegel R, Xu J, Ward E. Cancer statistics, 2010. CA Cancer J Clin. 2010; 60:277–300. [PubMed: 20610543]
2. Epstein, J.; Amin, M.; Reuter, V. Biopsy interpretation of the bladder. 2. Philadelphia, PA: Lippincott Williams & Wilkins; 2010.
3. Messing, E. Urothelial Tumors of the Bladder. In: Wein, AJ., editor. Wein: Campbell-Walsh Urology. 9. Vol. 3. PA: Saunders Elsevier; 2007.
4. Epstein, J.; Amin, M.; Reuter, V.; Mostofi, F. The World Health Organization/International Society of Urological Pathology Consensus Classification of Urothelial (Transitional Cell) Neoplasms of the Urinary Bladder. The American Journal of Surgical Pathology; The Bladder Consensus Conference Committee; 1998. p. 1435-1448.
5. Jones, S.; Campbell, S. Non–Muscle-Invasive Bladder Cancer (Ta, T1, and CIS). 9. Vol. 3. PA: Saunders Elsevier; 2007.

NIH-PA Author Manuscript

NIH-PA Author Manuscript

NIH-PA Author Manuscript


6. Lopez-Beltran A. Bladder cancer: clinical and pathological profile. Scand J Urol Nephrol Suppl. 2008:95–109. [PubMed: 18815924]
7. Pasin E, Josephson D, Mitra A, Cote R, Stein J. Superficial bladder cancer: an update on etiology, molecular development, classification, and natural history. Rev Urol. 2008; 10:31–43. [PubMed: 18470273]
8. Pan C, Chang Y, Chen K, Yu H, Sun C, Ho D. Prognostic significance of the 2004 WHO/ISUP classification for prediction of recurrence, progression, and cancer-specific mortality of non-muscle-invasive urothelial tumors of the urinary bladder: a clinicopathologic study of 1,515 cases. Am J Clin Pathol. 2010; 133:788–95. [PubMed: 20395527]
9. Williamson S, Montironi R, Lopez-Beltran A, Maclennan G, Davidson D, Cheng L. Diagnosis, evaluation and treatment of carcinoma in situ of the urinary bladder: The state of the art. Crit Rev Oncol Hematol. 2010; 76:112–26. [PubMed: 20097572]
10. Feifer A, Xie X, Brophy JM, Segal R, Kassouf W. Contemporary cost analysis of single instillation of mitomycin after transurethral resection of bladder tumor in a universal health care system. Urology. 2010; 76:652–6. [PubMed: 20394970]
11. Hall RR, Parmar MK, Richards AB, Smith PH. Proposal for changes in cystoscopic follow up of patients with bladder cancer and adjuvant intravesical chemotherapy. BMJ. 1994; 308:257–60. [PubMed: 8179678]
12. Denk W, Strickler J, Webb W. Two-photon laser scanning fluorescence microscopy. Science. 1990; 248:73–6. [PubMed: 2321027]
13. Zipfel W, Williams R, Christie R, Nikitin A, Hyman B, Webb W. Live tissue intrinsic emission microscopy using multiphoton-excited native fluorescence and second harmonic generation. Proc Natl Acad Sci U S A. 2003; 100:7075–80. [PubMed: 12756303]
14. Zipfel W, Williams R, Webb W. Nonlinear magic: multiphoton microscopy in the biosciences. Nat Biotechnol. 2003; 21:1369–77. [PubMed: 14595365]
15. Mukherjee S, Wysock J, Ng C, et al. Human bladder cancer diagnosis using Multiphoton microscopy. Proc Soc Photo Opt Instrum Eng. 2009; 7161 nihpa96839.
16. Rogart J, Nagata J, Loeser C, et al. Multiphoton imaging can be used for microscopic examination of intact human gastrointestinal mucosa ex vivo. Clin Gastroenterol Hepatol. 2008; 6:95–101. [PubMed: 18065276]
17. Yadav R, Mukherjee S, Hermen M, et al. Multiphoton microscopy of prostate and periprostatic neural tissue: a promising imaging technique for improving nerve-sparing prostatectomy. J Endourol. 2009; 23:861–7. [PubMed: 19425823]
18. White F, Gohari K, Smith C. Histological and ultrastructural morphology of 7,12 dimethylbenz(alpha)-anthracene carcinogenesis in hamster cheek pouch epithelium. Diagn Histopathol. 1981; 4:307–33. [PubMed: 6802623]
19. Taxy J. Frozen section and the surgical pathologist: a point of view. Arch Pathol Lab Med. 2009; 133:1135–8. [PubMed: 19642740]
20. Reddy G, Kelleher K, Fink R, Saggau P. Three-dimensional random access multiphoton microscopy for functional imaging of neuronal activity. Nat Neurosci. 2008; 11:713–20. [PubMed: 18432198]
21. Kim K, Buehler C, So P. High-speed, two-photon scanning microscope. Appl Opt. 1999; 38:6004–9. [PubMed: 18324120]
22. Saggau P. New methods and uses for fast optical scanning. Curr Opin Neurobiol. 2006; 16:543–50. [PubMed: 16962769]
23. Durst M, Zhu G, Xu C. Simultaneous spatial and temporal focusing for axial scanning. Opt Express. 2006; 14:12243–54. [PubMed: 19529653]
24. Howard, S.; Straub, A.; Xu, C. Multiphoton Modulation Microscopy for High-Speed Deep Biological Imaging. Conference on Lasers and Electro-Optics, OSA Technical Digest (Optical Society of America, 2010), paper CWD6; 2010.
25. Cauberg EC, de Bruin DM, Faber DJ, van Leeuwen TG, de la Rosette JJ, de Reijke TM. A new generation of optical diagnostics for bladder cancer: technology, diagnostic accuracy, and future applications. Eur Urol. 2009; 56:287–96. [PubMed: 19285787]

NIH-PA Author Manuscript

NIH-PA Author Manuscript

NIH-PA Author Manuscript


26. Lerner SP. Innovations in endoscopic imaging for bladder cancer. Eur Urol. 2009; 56:920–2. [PubMed: 19665285]
27. Motz JT, Fitzmaurice M, Miller A, et al. In vivo Raman spectral pathology of human atherosclerosis and vulnerable plaque. J Biomed Opt. 2006; 11:021003. [PubMed: 16674178]
28. Haka AS, Volynskaya Z, Gardecki JA, et al. In vivo margin assessment during partial mastectomy breast surgery using raman spectroscopy. Cancer Res. 2006; 66:3317–22. [PubMed: 16540686]
29. Low AF, Tearney GJ, Bouma BE, Jang IK. Technology Insight: optical coherence tomography--current status and future development. Nat Clin Pract Cardiovasc Med. 2006; 3:154–62. quiz 172. [PubMed: 16505861]
30. Schmidbauer J, Remzi M, Klatte T, et al. Fluorescence cystoscopy with high-resolution optical coherence tomography imaging as an adjunct reduces false-positive findings in the diagnosis of urothelial carcinoma of the bladder. Eur Urol. 2009; 56:914–9. [PubMed: 19674831]
31. Canto MI. Endomicroscopy of Barrett's Esophagus. Gastroenterol Clin North Am. 2010; 39:759–69. [PubMed: 21093753]
32. Wu K, Liu JJ, Adams W, et al. Dynamic Real-time Microscopy of the Urinary Tract Using Confocal Laser Endomicroscopy. Urology. 2011; 78:225–31. [PubMed: 21601243]
33. Chen M, Xu C, Webb W. Endoscope lens with dual fields of view and resolutions for multiphoton imaging. Opt Lett. 2010; 35:2735–7. [PubMed: 20717440]
34. Liu G, Xie T, Tomov I, et al. Rotational multiphoton endoscopy with a 1 microm fiber laser system. Opt Lett. 2009; 34:2249–51. [PubMed: 19649060]
35. Bao H, Gu M. A 0.4-mm-diameter probe for nonlinear optical imaging. Opt Express. 2009; 17:10098–104. [PubMed: 19506662]
36. König K, Weinigel M, Hoppert D, et al. Multiphoton tissue imaging using high-NA microendoscopes and flexible scan heads for clinical studies and small animal research. J Biophotonics. 2008; 1:506–13. [PubMed: 19343676]

NIH-PA Author Manuscript

NIH-PA Author Manuscript

NIH-PA Author Manuscript

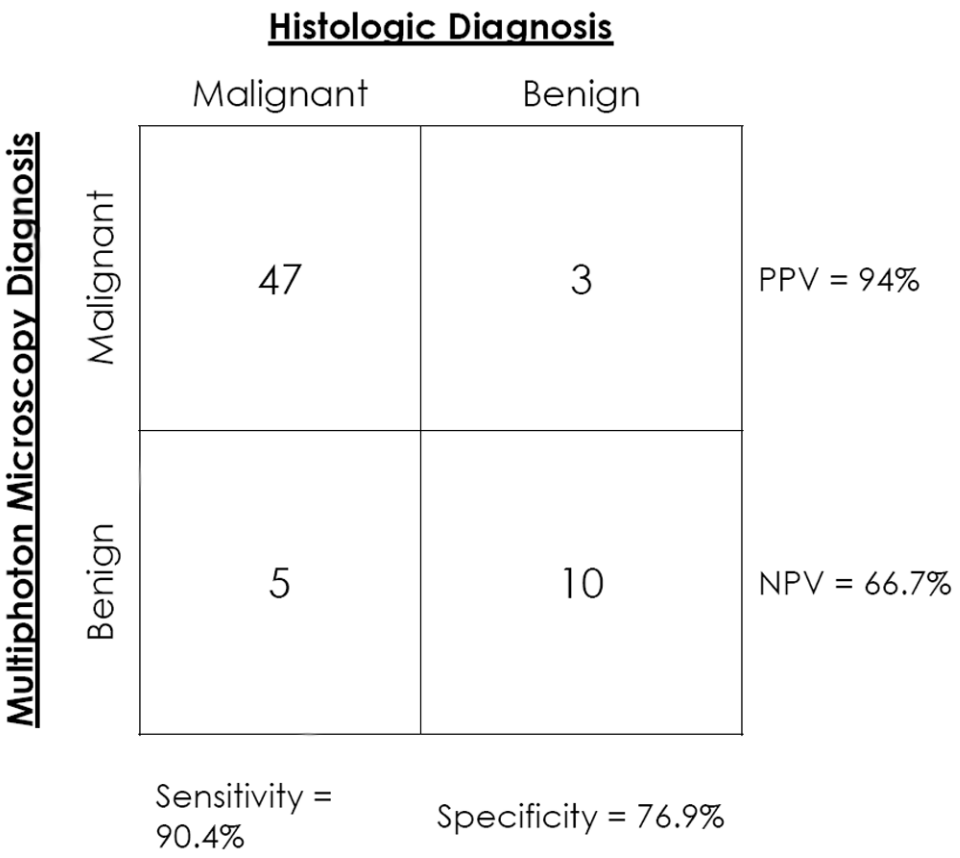


**Fig 1. A 2 × 2 contingency table comparing multiphoton microscopy diagnosis with the final histopathologic diagnosis**

Abbreviations: PPV - positive predictive value; NPV - negative predictive value

NIH-PA Author Manuscript

NIH-PA Author Manuscript

NIH-PA Author Manuscript

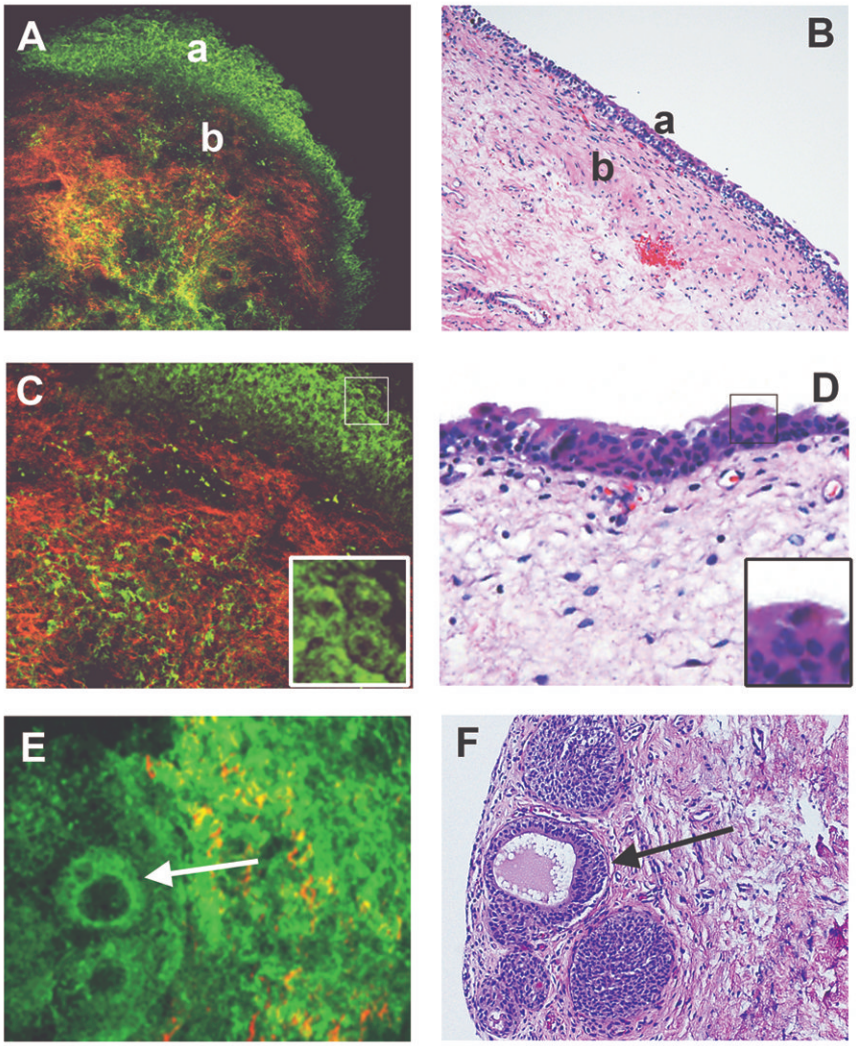


**Fig 2. Normal structures of bladder wall and flat intraurothelial lesions without atypia**

Multiphoton microscopy (MPM) image (**A**) and corresponding H&E image (**B**) at low magnification showing clear demarcation between normal urothelium (*a*) and lamina propria (*b*). Lamina propria is composed of collagen bundles (red) and elastin fibers (green). MPM image (**C**) and corresponding H&E image (**D**) at high magnification showing multi-layered urothelium and superficial umbrella cells. Umbrella cells in each image are boxed and shown at higher digital zoom in the inset. MPM image (**E**) and corresponding H&E image (**F**) at low magnification showing von Brunn nests, some with cystic dilatation (*cystitis cystica*; arrow). (MPM magnifications: A=120X, C=240X, E=306X;H&E magnifications: B=40X, D=200X, F=200X).

NIH-PA Author Manuscript
NIH-PA Author Manuscript
NIH-PA Author Manuscript



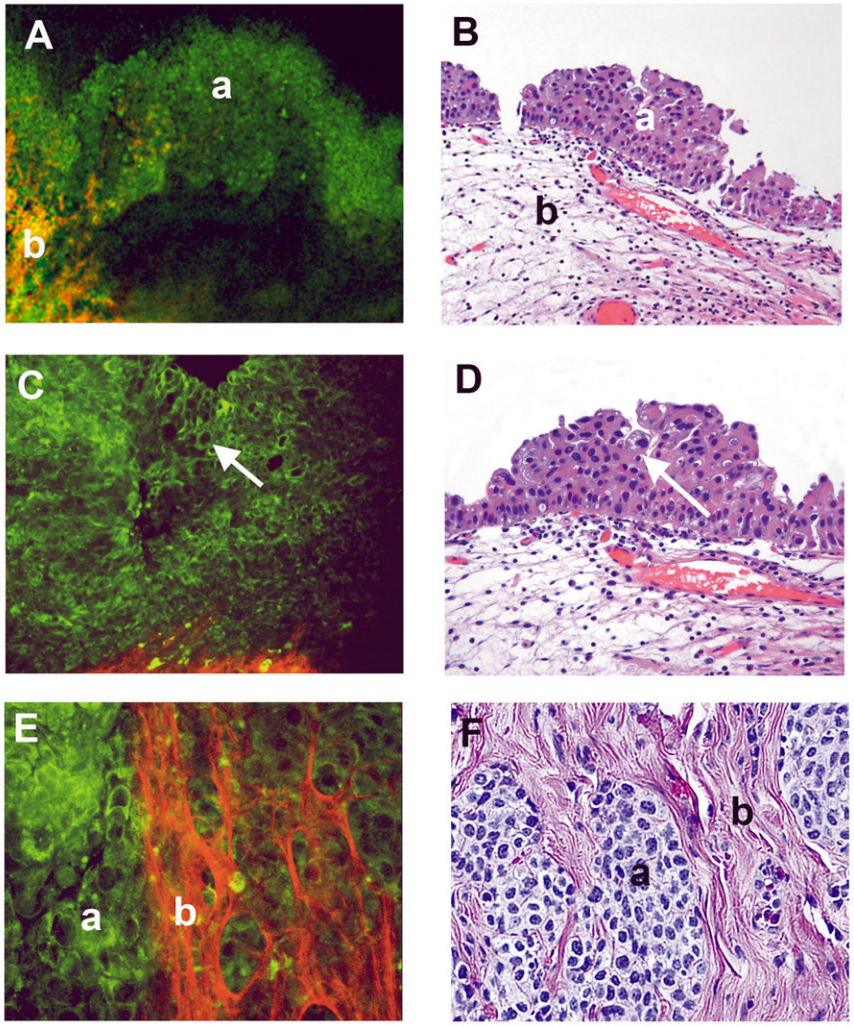


**Fig 3. Carcinoma *in situ* (CIS) and invasive urothelial carcinoma**

Multiphoton microscopy (MPM) image (**A**) and the corresponding H&E image (**B**) at low magnification showing flat urothelium with loss of polarity (*a*) and underlying lamina propria (*b*). MPM image (**C**) and corresponding H&E image (**D**) at high magnification showing high grade cytologic features [marked pleomorphism and increased Nuclear:Cytoplasmic (N:C) ratio; arrow]. MPM image (**E**) and corresponding H&E image (**F**) at high magnification showing nests of invasive tumor cell (*a*; color-coded green) in collagen fibers of lamina propria (*b*; color-coded red). (MPM magnifications: A=48X, C=293X, E=480X; H&E magnifications: B=40X, D=200X, F=400X)

NIH-PA Author Manuscript
NIH-PA Author Manuscript
NIH-PA Author Manuscript



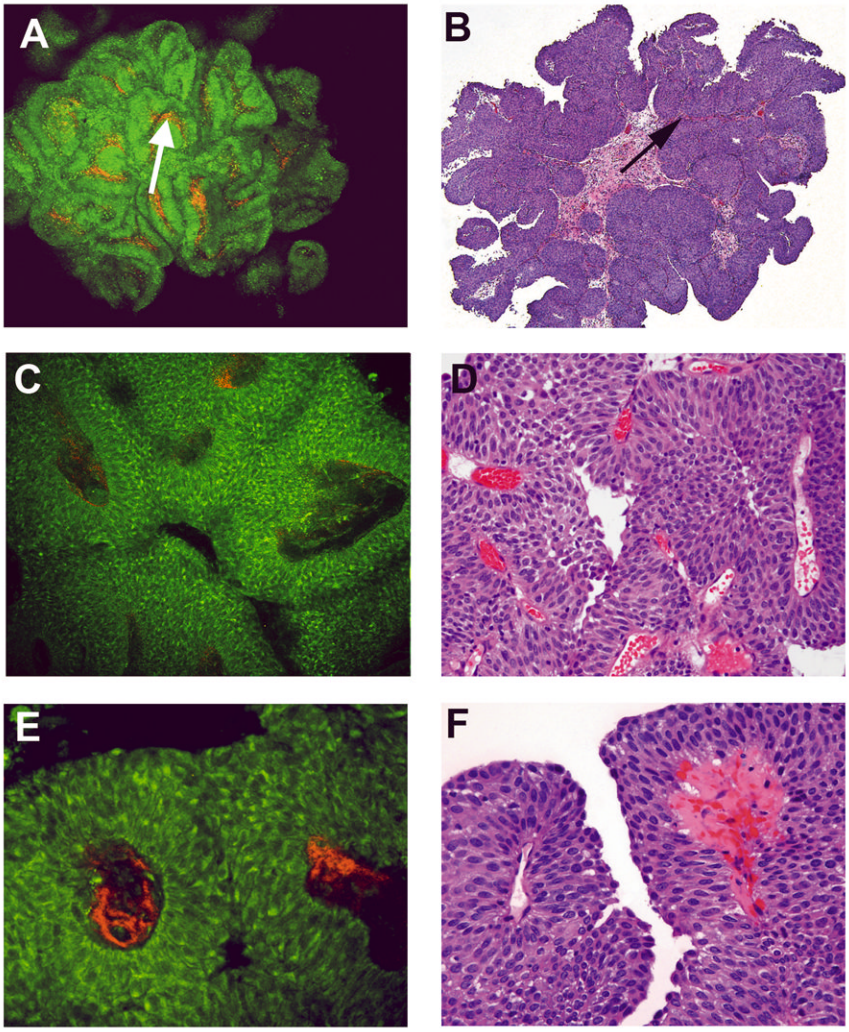


**Fig 4. Papillary urothelial carcinoma, low grade, non-invasive**

Multiphoton microscopy (MPM) image (**A**) and corresponding H&E image (**B**) at low magnification showing the papillary nature of the lesion (complex papillae with thin fibrovascular cores; arrow). MPM image (**C**) and corresponding H&E image (**D**) at high magnification showing thin fibrovascular cores (arrow). MPM image (**E**) and corresponding H&E image (**F**) at high magnification showing thickened urothelium lined by cells with minimal pleomorphism and relatively low Nuclear:Cytoplasmic (N:C) ratio. MPM magnifications: A=48X, C=240X, E=480X; H&E magnifications: B=40X, D=200X, F=400X)

NIH-PA Author Manuscript
NIH-PA Author Manuscript
NIH-PA Author Manuscript



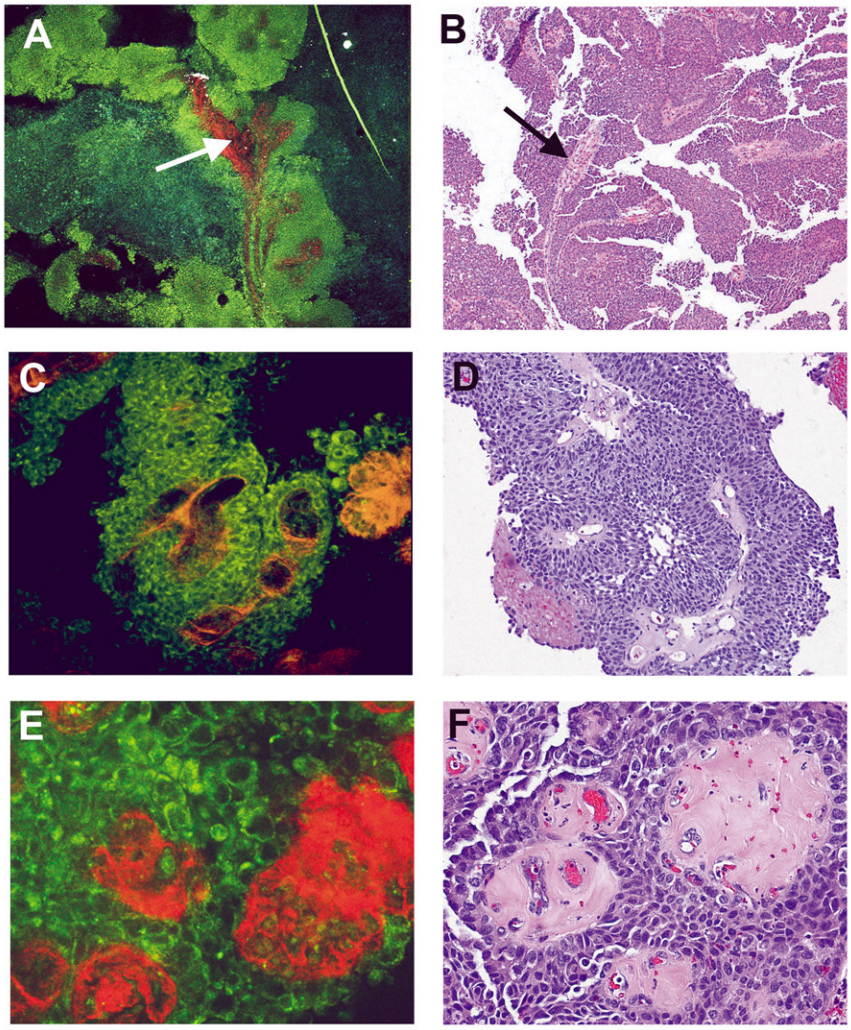


**Fig 5. Papillary urothelial carcinoma, high grade, non-invasive**

Multiphoton microscopy (MPM) image (**A**) and corresponding H&E image (**B**) at low magnification showing the papillary nature of the lesion (complex, thickened papillae with thin fibrovascular cores; arrow). MPM image (**C**) and corresponding H&E image (**D**) at high magnification showing thickened fibrovascular cores and disorderly arrangement of cells. MPM image (**E**) and corresponding H&E image (**F**) at high magnification showing cells with marked pleomorphism, high Nuclear:Cytoplasmic (N:C) ratio, and hyalinized fibrovascular cores. MPM magnifications: A = 48X, C = 240X, E = 480X; H&E magnifications: B=40X, D=200X, F=400X).

NIH-PA Author Manuscript
NIH-PA Author Manuscript
NIH-PA Author Manuscript



## Table 1

Comparative features between Hematoxylin-Eosin (H&E) and Multiphoton Microscopy (MPM) for evaluation of human bladder biopsies.

| | Diagnostic features identifiable on both H&E and Multiphoton microscopy (MPM) | Multiphoton microscopy (MPM) limitations |
|---|---|---|
| **Benign, flat intraurothelial lesions** | **1** Multilayered urothelium with superficial umbrella cells<br>**2** Maintained cell polarity<br>**3** Underlying lamina propria with blood vessels, von Brunn nests | Lack of intranuclear details |
| **Carcinoma *in situ* (CIS)** | **1** Flat lesion<br>**2** Marked pleomorphism<br>**3** High nuclear:cytoplasmic (N:C) ratio<br>**4** Loss of polarity | Lack of intranuclear detail may impair ability to distinguish CIS from urothelial dysplasia or reactive urothelium |
| **Low grade papillary urothelial carcinoma** | **1** Papillary fronds with thin fibrovascular cores<br>**2** Overall orderly arrangement of urothelial cells with mild pleomorphism<br>**3** Relatively low Nuclear:Cytoplasmic (N:C) ratio | Difficult to differentiate between papilloma, papillary urothelial neoplasms of low malignant potential (PUNLMP) and low grade papillary urothelial carcinoma |
| **High grade papillary urothelial carcinoma** | **1** Papillary fronds and occasional sheets of tumor cells<br>**2** Moderate to marked nuclear and cellular pleomorphism<br>**3** High Nuclear:Cytoplasmic (N:C) ratio<br>**4** Loss of polarity | Lack of intranuclear detail may impair ability to distinguish high grade from low grade lesions |
| **Invasive urothelial carcinoma** | Irregular nests of tumor cells, or individual tumor cells, within lamina propria (pT1) or muscularis propria (pT2) | **1** Invasion reliably identified only if extensive; microinvasion not easily identified<br>**2** Difficult to assess muscularis propria presence, including involvement by tumor, due to penetration depth limitation in current Multiphoton microscopy (MPM) imaging instrumentation |